Syst. Zool., 35(3):381-399, 1986

FINITE-ELEMENT SCALING APPLIED TO SEXUAL DIMORPHISM IN RHESUS MACAQUE (*MACACA MULATTA*) FACIAL GROWTH

JAMES M. CHEVERUD AND JOAN T. RICHTSMEIER

Departments of Anthropology and of Cell Biology and Anatomy, Northwestern University, Evanston, Illinois 60201

Abstract.—While many advances have been made in the statistical treatment of morphometrics, there has been little improvement in the design of measurements subjected to statistical analysis. Commonly measured linear dimensions result in a loss of geometrical integrity and an inability to translate multivariate statistical results into material three-dimensional morphology. Problems with the definition of size and shape, spurious correlation, and anatomical localization of form change or difference arise with linear dimensions. Finite-element scaling methods overcome these problems and produce measures that can be subjected to standard multivariate statistical analyses. The finite-element scaling method is described, as are measures of local and general size and shape change. We use finite-element scaling as a basis for an analysis of sexual dimorphism in rhesus macaque (*Macaca mulatta*) facial growth. Males grow approximately twice as fast as females, although facial growth stops at nearly the same age in the two sexes. The adult female face is morphologically quite similar in all aspects of size and shape to that of a juvenile male (4.5 years old). Thus, considered heterochronically, and taking the female morphology as primitive, sexual dimorphism in the size and shape of the rhesus face arose through rate hypermorphosis. Growth of the face was strongly allometric, with the maxillary alveolus growing much faster than other facial regions. Finite-element scaling is a very useful measurement tool for the comparison of forms, especially in studies of growth and phylogenetic transformation. [Finite-element scaling; *Macaca mulatta*; rhesus macaque; sexual dimorphism; facial growth.]

Modern morphometric methods are centered on the multivariate statistical analysis of measurements taken on the study objects. Many advances and much sophistication in statistical technique has been gained since the foundation of biometric science in the late 19th century. However, there has been little gain in measurement-design sophistication. Typically, some standard set of linear distances, angles, and volumes is recorded with little consideration of whether these are optimal for the comparison to be made or how comparisons can be interpreted. The measurements taken usually have the sanction of tradition, allowing comparison of a new study with a previous body of work. As Karl Pearson noted over 60 years ago,

> The ... great difficulty of the craniologist lies in the measurements he proposes to take. He is burdened by the past history of his science. If he neglects the past history of his science and adopts new and possibly better characters for record, he cuts himself off from the possibility of forming comparisons with a wide range of measurements on innumerable races already made [Pearson and Davin, 1924:329].

This phenomenon has resulted in a historical inertia limiting innovation in measurement techniques, while the statistical methods used to analyze these measurements have progressed apace.

In this paper, we describe a relatively new method of morphological measurement, finite-element scaling (Lewis et al., 1980; Cheverud et al., 1983; Richtsmeier, 1985; Richtsmeier and Cheverud, 1986), and apply it to a comparative analysis of facial growth in male and female rhesus macaques (*Macaca mulatta*). This measurement method uses two- or three-dimensional point coordinates to describe individual forms and produces a variety of physically-based measurements to describe the differences between forms. Thus, finite-element scaling is within the tradition of measurement first suggested by Thompson (1917). While Thompson's method of coordinates has always had in-

tuitive appeal to morphologists as an economical, visual way to compare forms, it has not often been used, due to the fact that Thompson gave no detailed instructions on how to proceed with his method or how to mathematically define his complex mappings of one form into another. They were also two-dimensional representations of three-dimensional forms. The method was analytically unwieldy (Medawar, 1958) and did not lead directly to the now familiar multivariate statistical analyses used to test hypotheses. Recently, McMahon and Bonner (1983:25) have repeated these criticisms,

> One difficulty is that it [Thompson's method] depends upon two-dimensional representations of three-dimensional objects. But, the main problem grows out of its principal virtue: it is a way of visualizing many changes at once, and it becomes exceedingly difficult and impractical to assign numerical values to those continuously changing grid lines.

Despite the difficulties, there have been many attempts over the past 70 years to follow up and advance Thompson's approach to measurement. These are reviewed in Bookstein (1978). Especially notable are Lestrel's (1974) work with Fourier analysis and Sneath's (1967) biological application of trend-surface analysis. Most recently and successfully, Bookstein (1978, 1983, 1984a; Grayson et al., 1985) introduced biorthogonal grid analysis and has begun work on finite-element methods. In addition to our own work in finite-element scaling (Lewis et al., 1980; Cheverud et al., 1983; Richtsmeier, 1985; Richtsmeier and Cheverud, 1986), a similar approach has been suggested by Moss and Skalak (Skalak et al., 1982; Moss, 1983; Patel, 1983; Moss et al., 1985). The finite-element scaling approach allows a positive response to critics of Thompson's method of coordinates.

PROBLEMS WITH LINEAR DIMENSIONS

Finite-element scaling solves several problems related to the use and interpretation of comparisons between forms made with linear dimensions and angles—problems that are severe enough in many instances to warrant abandoning traditional measurement systems. The central problems revolve around a loss of geometry from the analysis and an inability to specify the location of form differences.

Linear dimensions abstracted from a form typically result in a loss of geometrical integrity. When distances between landmarks are measured, the magnitudes, but not directions, of these linear distances are typically recorded. It is impossible to reconstruct the relative landmark positions, or geometrical form, from all but a very specialized set of linear dimensions. It is much more efficient to record the two- or three-dimensional coordinates of landmarks as a map or model of the object being studied. This map can then be used in finite-element scaling or to calculate linear dimensions between landmarks. Statistical analysis of linear dimensions is relatively straightforward, but produces morphologically difficult results in that they cannot be easily translated from statistical n-space into three- or two-dimensional morphological space. Material forms are three-dimensional, not 10- or 20-dimensional, and ideally our analyses should be interpretable in terms of material three-dimensional morphology. Strictly, this is not possible with linear dimensions as measurements (but see Strauss and Bookstein [1982] for an exceptional case).

Definitions of size and shape in relation to form are also quite difficult with systems of linear measurements (Gould, 1966; Mosimann, 1970; Sprent, 1972; Mosimann and James, 1979; Bookstein et al., 1985). Traditionally, form is conceived as being decomposable into size and shape components to the extent that form = size + shape (Sprent, 1972). However, the possibility of separate size and shape measurement has led to much discussion and controversy. We believe this is due to inconsistency between our intuitive geometrical conceptions of size as magnitude and shape as spatial variation in magnitude, and common statistical reifications of these concepts. Size and shape should be defined in three-dimensional morpho-

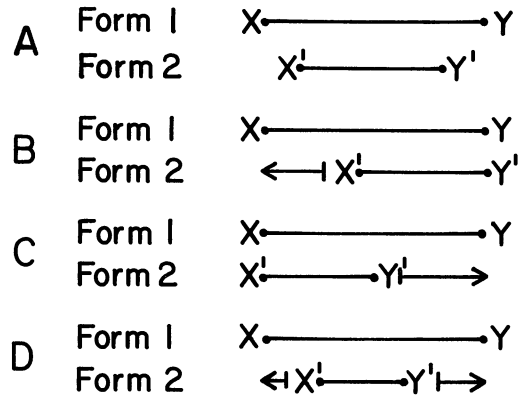

FIG. 1. Difficulties occur in locating differences which result in form 1 being longer than form 2: (A) linear dimensions XY in forms 1 and 2; (B) difference in XY length due to differences local to X; (C) difference in XY length due to differences local to Y; (D) difference in XY length due to differences at both points X and Y (after Enlow [1975] and Bookstein [1983]).

logical space rather than n-dimensional statistical space. Multivariate statistical analyses can then be pursued on measures interpretable in three-dimensional morphological space.

The use of linear dimensions can also lead to spurious, geometrically necessary correlations between traits, thus making studies of morphological integration difficult to interpret. It can be shown, analytically or by computer simulation, that when two linear dimensions share a common point, the correlation between these two measurements is a function of the angle between them even when the points' positions vary independently and randomly. When all three points forming an angle vary, the correlation (r) between the two linear dimensions is

$$r = (\tfrac{1}{2})\cos\theta, \qquad (1)$$

where θ is the average angle between the two linear dimensions. If the angle is less than 90°, a positive spurious correlation results; if it is greater than 90°, a negative spurious correlation results. Only measurements at 90° angles are free of such spurious correlation ($\cos 90° = 0$). "They are not true organic correlations, but to a large extent result from what we may term mathematical necessity" (Pearson and Davin, 1924:349). Thus, a morphometric correlation matrix may reflect the arbitrary geometry of the linear dimensions as well as the biological relationships among the landmarks defining the linear dimensions.

A related and even more serious problem arises in interpreting the locus of morphological difference or change when comparing linear dimensions from two or more forms. Consider the linear dimension between landmarks X and Y (see Fig. 1; Enlow, 1975; Bookstein, 1983). This dimension is longer in form 1 than in form 2, but we have no information on why it is longer. Material may have been added at point X with no change at point Y (Fig. 1b); all of the change might have occurred at point Y (Fig. 1c); change may have occurred at both points (Fig. 1d); points X and Y may have been relocated due to changes at some distant locus. In comparing linear dimensions you can only say that one point moves *relative* to another, but this may mask a wealth of variability in the causes of Y's relocation relative to X.

This inability to localize changes or differences between two forms is a special case of the registration problem in roentgenographic cephalometry (Richtsmeier and Cheverud, 1986). In such studies, cephalic X-rays are superimposed or registered one upon another using a common origin (often at point sella, the center of sella turcica) and line of orientation (often sella to nasion). All of the other landmarks are then described as moving relative to the origin and orientation line. While this provides a consistent description, it does not allow identification of the locus of morphological difference between the two forms compared (Enlow, 1975; Moyers and Bookstein, 1979; Moss et al., 1980; Skalak et al., 1982; Cheverud et al., 1983; Moss, 1983; Richtsmeier, 1985; Richtsmeier and Cheverud, 1986). All measurements taken in a registered system, including linear dimensions, are *observer inherent* (Cheverud et al., 1983) in that their interpretation depends entirely on the position of the ob-

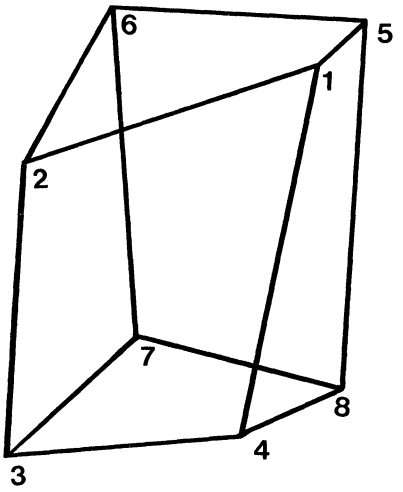

FIG. 2. Single finite element from the neurocranium. It is an eight-noded hexahedron.

server relative to the objects studied and not on the objects themselves. On a cosmic scale it is obvious to us on Earth that the sun rises and sets, our position remaining constant. This is due to the incorrect, but obvious, interpretation of observer-inherent measures of the sun's location and movement relative to our own. In morphometrics, *object-inherent* measurements are needed so that we can separate our perceptions from the behavior of the system being observed.

Finally, the same set of linear dimensions is often used for a multiplicity of comparisons, between sexes, between species or populations, etc. However, different sets of measurements may often best describe diverse contrasts between forms. While multivariate statistical techniques, such as discriminant function analysis, may define the linear combination of an arbitrary set of dimensions which best discriminates between groups, the measurements themselves may be poor discriminators relative to some other, unmeasured set. It is likely that the best measurements for contrasting species A with species B will not be the same as those contrasting species A with species C. Thus, we would need to remeasure samples for each contrast of interest in order to optimally discriminate between forms, even though we would have no a priori knowledge of which measurements to take. Recording traditional measurements and using them for all kinds of comparisons is not a solution to this general problem.

We have detailed several problems with the use of linear dimensions and the interpretation of comparisons based on them. Chief among these are registration problems including the inability to localize morphological differences (observer inherence) and spurious correlation. We feel that the problems are severe enough to warrant considering alternative forms of measurement that are free from these lethiferous ills. Thus, we turn our attention to finite-element scaling.

FINITE-ELEMENT SCALING

Finite-element scaling is a method of comparison that overcomes these problems, in that it: (1) retains the three-dimensional nature of physical form in its measurements but still allows standard multivariate statistical analyses for hypothesis testing; (2) provides for the separate measurement of geometrically defined size and shape components of form change; (3) provides measures at 90° to one another, thus, eliminating geometrically-based spurious correlation; (4) provides both localized and summary measures of form differences; (5) is registration-free in that it registers simultaneously on every point, thus providing object-inherent measurements; and (6) defines the *measurements* which best differentiate among the forms compared.

The method is based on principles of finite-element analysis and continuum mechanics. For this application, it was developed by Lewis et al. (1980) and elaborated by Cheverud et al. (1983); these sources should be referenced for a more detailed description of the mathematics upon which the approach rests. Bookstein's (1978, 1983, 1984a) methods are one version of finite-element scaling. Our method differs from his in being three-dimensional and nonhomogeneous, meaning that each point within the object

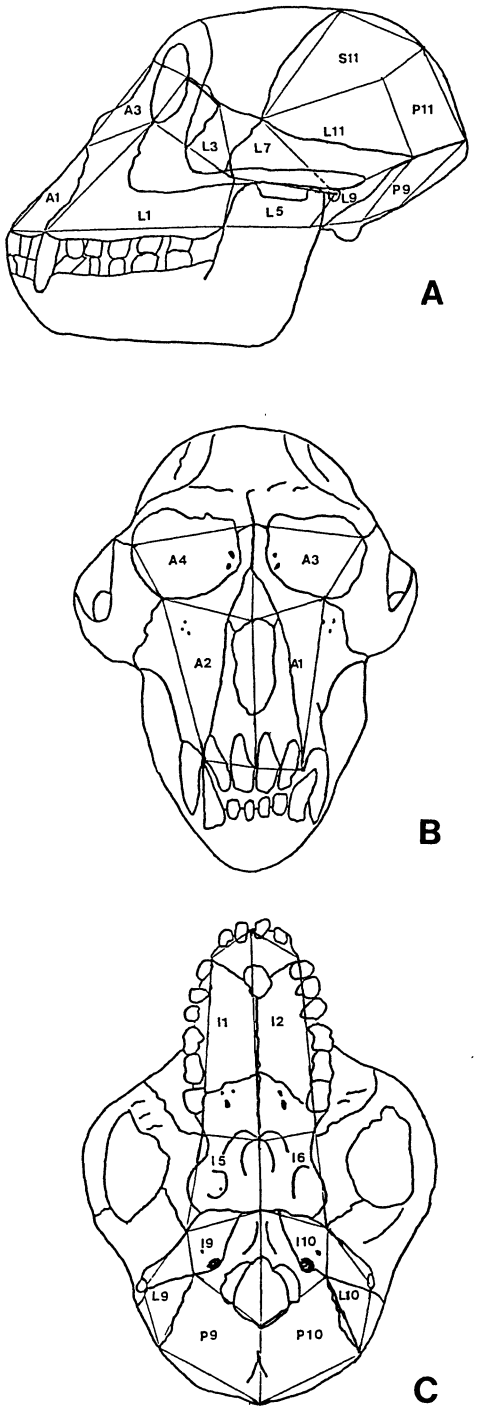

FIG. 3. (a) Lateral, (b) anterior, and (c) inferior views of elements modelling a rhesus macaque skull. Element faces numbered 1 to 12 and anterior (A), lateral (L), superior (S), posterior (P), and inferior (I) aspects of an element are indicated by appropriate letter (elements defined in and figure drawn after Cheverud et al. [1983]).

may have its own local deformation rather than all points having the same deformation, as in a homogeneous method. However, these differences are a matter of detail, not general approach.

Finite elements.—A finite-element analysis begins with the three-dimensional coordinates of a series of landmarks reliably located on the forms of interest. The results are most easily interpreted if biologically homologous landmarks are used rather than extremal points or points whose definition depends on some arbitrary registration system, such as the Frankfort horizontal. Moyers and Bookstein (1979) and Bookstein (1984b) provided discussions concerning landmark choice. Once three-dimensional point coordinates are obtained, the object (e.g., a skull) is divided into several finite elements. In our current applications, a finite element is a bounded eight-noded hexahedron (cubelike) with vertices (or corners) composed of biologically homologous points. An example of a single element is given in Figure 2. The vertices are connected by straight lines. The more cubelike the element, the more accurate the measured comparison. Long, narrow hexahedra can produce unreliable results and may twist on themselves producing a mathematical singularity and preventing finite-element analysis (Lewis et al., 1980).

The objects to be analyzed are divided into several elements which are then used as approximate models of the forms themselves. We have divided the rhesus macaque cranium into 12 elements (6 per side) as shown in Figure 3. While the definition of elements is arbitrary, it is desirable to restrict elements to relatively homogeneous areas of growth or form difference. Some element configurations may be more useful than others for particular comparisons. While we describe finite-element scaling with three-dimensional hexahedra, the method is much more general and

flexible, encompassing a myriad of geometrical forms including triangles (Bookstein, 1983, 1984a; Moss et al., 1985) and tetrahedra (Lew and Lewis, 1977).

Homology functions.—Once finite elements are defined, the analysis proceeds one element at a time. Two forms are considered, a reference form and a homologous target form. Finite-element analysis compares an element in the reference object to one in the target object. It does not measure individuals, who are defined by the coordinates of landmarks, but rather measures the deformation of one object into another. Thus, it measures contrasts.

As in all geometric methods, finite-element scaling relates every point within the reference element to a "homologous" point in the target element using a homology function. The homology function is the key to finite-element scaling. For every point upon or inside of the reference element, the homology function defines its homologue in the target element. This form of homology is defined by the homology function, not by strict biological criteria (Riedl, 1978). Ideally, the homology function is derived or defined using biological homology so that biologically homologous points are also identified as "homologous" by the function. Homological relationships for all other points are interpolated using the homology function derived from the known points. Thompson (1917) noted that some of his homology functions, such as that used in the famous porcupine fish (*Diodon* sp.) to sunfish (*Orthagoriscus mola*) deformation, were flawed in that biologically homologous points did not map perfectly one-on-one. Rather, Thompson's functions modeled the deformation with fair, but not perfect accuracy.

In our application of finite-element scaling, the homology function is computed using the homologous landmarks that are the vertices of the element so that these biologically homologous vertices are perfectly mapped. The homology of points internal to the element are determined by interpolation using the homology function derived from the known points and, thus, are subject to error. The more spatially restricted the element, the more accurate the mapping of internal points.

TABLE 1. Homology functions for the eight vertices of a hexahedral finite element (Lewis et al., 1980) calculated from equations 3 and 4.

Vertex	Normalized coordinates	h_a
1	(1, 1, 1)	$(\frac{1}{8})(1 + r)(1 + s)(1 + t)$
2	(1, 1, −1)	$(\frac{1}{8})(1 + r)(1 + s)(1 - t)$
3	(1, −1, −1)	$(\frac{1}{8})(1 + r)(1 - s)(1 - t)$
4	(1, −1, 1)	$(\frac{1}{8})(1 + r)(1 - s)(1 + t)$
5	(−1, 1, 1)	$(\frac{1}{8})(1 - r)(1 + s)(1 + t)$
6	(−1, −1, 1)	$(\frac{1}{8})(1 - r)(1 - s)(1 + t)$
7	(−1, 1, −1)	$(\frac{1}{8})(1 - r)(1 + s)(1 - t)$
8	(−1, −1, −1)	$(\frac{1}{8})(1 - r)(1 - s)(1 - t)$

The functions used here are

$$X_i = \sum_{a=1}^{8} h_a X_{ai}, \qquad (2)$$

where X_i is the X, Y, or Z coordinate of some point of interest in the reference element, X_{ai} represents the corresponding coordinate for one of the eight vertices in the reference element, and h_a is the homology function solution for that vertex (see Table 1). Point locations (X_i and X_{ai}) are known, while h_a is estimated. This function maps points from an observed element, defined in the X-Y-Z-space, into a standardized cube with corresponding r, s, and t axes, each of unit length in positive and negative directions (see Fig. 4). The coordinates of the vertices (b_a) in the standardized cube can only take on values of +1 or −1 (for example, [1, 1, −1], [1, −1, 1], etc.). Points with the same r, s, and t normalized coordinates are defined as "homologous" by the homology function.

The homology function value for a given vertex, a, and point of interest, X, is

$$h_a = \mathrm{H}(r, r_a)\mathrm{H}(s, s_a)\mathrm{H}(t, t_a), \qquad (3)$$

where r, s, and t are the standardized coordinates (b) of the point of interest, r_a, s_a, and t_a are the standardized coordinates of vertex a, and H refers to the function,

$$\mathrm{H}(b, b_a) = (\tfrac{1}{2})(1 + bb_a), \qquad (4)$$

and b stands for the r, s, or t coordinate value. The particular homology-function

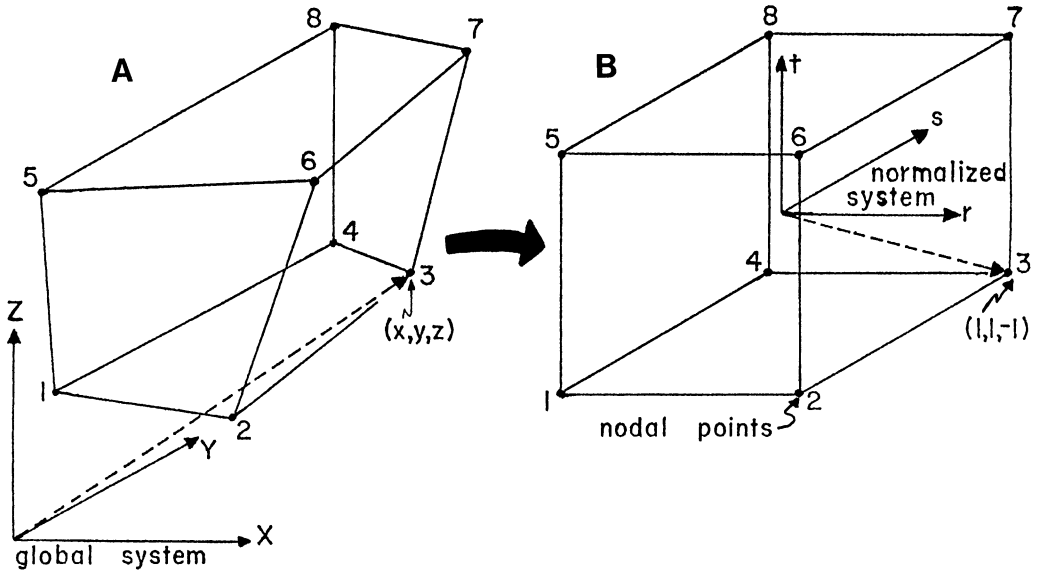

FIG. 4. Homology function maps points from observed reference element into a standardized cube. Points with same coordinates in standardized space are homologous (after Lewis et al. [1980]).

values for the eight nodal points are given in Table 1. In general, the values of r, s, and t are estimated from equation 2, solving for r, s, and t with prescribed values of X_i and X_{ai}.

For the centroid and vertices of an element, the equations in Table 1 are very easy to solve. The centroid has standardized coordinates of (0, 0, 0) and when these values are inserted into the equations in Table 1 and equation 2,

$$X_i = \left(\sum_{a=1}^{8} X_{ai}\right)/8. \tag{5}$$

The coordinates of the centroid are the average coordinates of the eight vertices. The vertices also show simplified functions. For vertex 1 with normalized coordinates of (1, 1, 1), equation 2 becomes

$$X_i = X_{1i}. \tag{6}$$

Since, by definition, points with the same r, s, and t coordinates are homologous, the location of point X' in the target element, which is the homolog of point X in the reference element, can be determined,

$$X'_i = \sum_{a=1}^{8} h_a X'_{ai}, \tag{7}$$

where the h_a are those produced by solving equation 3 in the reference element, the X'_{ai} are the measured vertex coordinates in the target object, and X'_i is unknown. Using this, we can map any point in the reference element into the target element in a manner consistent with known biological homology.

We have used this procedure to produce Thompson grids (Cheverud et al., 1983) as in the deformation of a one-year-old male into an adult male rhesus macaque skull (Fig. 5). A square grid was placed on the one-year-old male and the positions of crossing axes recorded. These internal points then were mapped, using the procedure described above, from the one-year-old male (reference elements) to an adult male (target elements) and the axes redrawn through the points. Point locations outside of the skull outlines are unreliable. While the analysis was performed three-dimensionally, only a sagittal section is displayed to relieve the observer's eye.

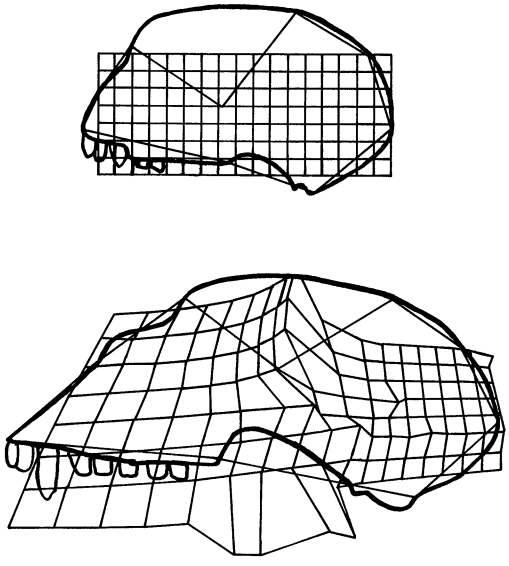

FIG. 5. Thompson grid displaying deformation of a one-year-old male into average adult male skull. Comparable points in grid are homologous, as defined by homology functions of elements. Outlines of rhesus crania placed on grid for purposes of orientation and do not represent scaled points. Display is in only two dimensions (although deformation was in three) to relieve the viewer's eye (after Cheverud et al. [1983]).

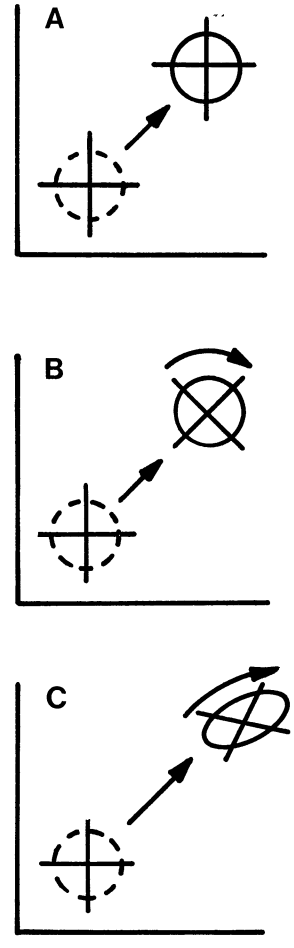

FIG. 6. (A) Rigid body displacement, plus (B) rigid body rotation, and (C) two-dimensional stretching of material immediately surrounding point of interest. Provides a complete description of morphological changes occurring during deformation. Dashed circle is original position and configuration.

Strain measurement.—While Thompson grids provide a convenient, eye-catching, graphic describing the deformation of one form into another, it will be necessary to derive a numerical description of the deformation in order to perform statistical analyses. Such a description is derived from the principles of continuum mechanics (Malvern, 1969) in terms of strain. We use strain here simply as a metric of form difference specific to a point, not as a measure of strain due to the imposition of physical force on a continuously distributed, but nongrowing material. Thus, our measures are not attempts to define the physical forces that generate growth, merely a convenient metric to measure differences or changes in form.

When a continuum is deformed, the material immediately surrounding each point in the reference element will undergo a rigid body displacement, rigid body rotation, and three-dimensional stretching (see Fig. 6). Lewis et al. (1980) described the measurement of deformation in some detail. The rigid body motion—displacement and rotation—of a given point can be calculated. Thus, points can be seen to move relative to one another as measured by standard linear dimensions. However, by their nature, measures of rigid body motion are observer inherent, or depend on the spatial relationships between the observer and the object, and the quantitative and qualitative results obtained de-

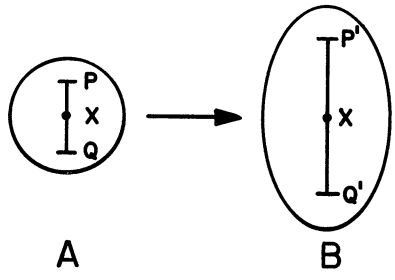

FIG. 7. Finite-element measurement of strain: (A) original configuration; (b) deformed configuration (see text for explanation).

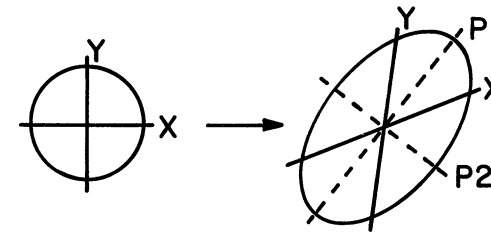

FIG. 8. Principal coordinates system describing strain local to a point. First principal direction (P1) defines the dimension of greatest strain, while second (P2) and third principal directions describe consecutively less strain in directions orthogonal to P1.

pend on a specific system of registration. Rigid body displacement and rotation of a point are due to forces that are external to the region immediately surrounding it. A region immediately surrounding a point may not deform at all in the transformation of one object into another, but the point may still be displaced. Thus, measurements of rigid body motion do not necessarily relate to localized differences and retain most of the problems of linear dimensions described above.

We choose instead to concentrate on the object-inherent measures of three-dimensional stretch, or strain, local to a given point. Such a descriptor allows one to determine the locus or loci of difference between forms. The basic descriptor of local deformation is the form tensor **F** (called the Lagrangian strain tensor in continuum mechanics), which mathematically describes an ellipsoid. It is a three-by-three symmetric matrix,

$$\mathbf{F} = \begin{bmatrix} n_x & e_{xy} & e_{xz} \\ e_{yx} & n_y & e_{yz} \\ e_{zx} & e_{zy} & n_z \end{bmatrix}, \qquad (8)$$

with the normal strains (n_i) along the diagonal and shear strains (e_{ij}) off-diagonal. This tensor describes the deformation of a sphere immediately surrounding the point of interest in the reference element into its ellipsoid shape in the target element (see Fig. 6). The normal strains measure stretch along the specified axis (X, Y, Z) and indicate the extent to which an infinitely short line element parallel to the ith axis increases or decreases its length in going from the reference to the target element. The shear strains record the change in angle between the specified axes in going from the reference to the target element.

One can think of finite-element scaling as measuring strain in the following way (see Fig. 7). Some point of interest, X, is chosen in the reference element. Points P and Q are arbitrarily chosen along some line passing through X and are equidistant from X. In practice, line segment PQ is infinitely short. The homology function values are derived for points P and Q in the reference element (equations 2–4). These are then used to locate P' and Q' in the target element (equation 7). Strain is defined as the difference between PQ's length in the target and reference elements, relative to its length in the reference,

$$\text{Strain} = [(P' - Q') - (P - Q)] \div (P - Q). \qquad (9)$$

Since PQ's length is infinitely short, finite-element scaling produces scale-free strain measurements which can be compared from one element to another and from one deformation to another. The form tensor mathematically summarizes the strain in all directions (all line segments PQ) at the specified point of interest. Thus, it retains the geometry of form in its measurement of differences between forms.

The form tensor values change quantitatively depending on the specific coordinate system used to define the reference

element. However, tensors describing the same deformation in different coordinate systems are mathematically equivalent in that simple tensor rotations relate one to another. Thus, the form tensor is an object inherent measure. While tensors described in all coordinate systems are mathematically equivalent, a convenient one is the principal coordinate system in which all strain is normal and none is shear. This coordinate system is defined by the eigenvectors of the form tensor, the associated eigenvalues (λ) giving the magnitude of normal strain in the principal directions (see Fig. 8). The mathematical operation described here is the same as that performed in principal components analysis in n-dimensional statistical space, but here form is described in material morphological space. Measuring strain in the principal coordinates system has several advantages. (1) The first eigenvector, associated with the eigenvalue with the largest absolute value, is the linear dimension along which the two forms being compared are most different. It is the best discriminating measurement between the forms. (2) All measurements sharing a common point are at 90° angles to one another, thus eliminating geometrically-based spurious correlation. (3) The eigenvalues can be used to calculate several invariants of the deformation (see below).

The form tensor can be divided into two additive components (see Fig. 9): a size tensor (**S**, often called the Spherical strain tensor); and a shape tensor (**T**, often called the Deviatoric strain tensor),

$$\mathbf{F} = \mathbf{S} + \mathbf{T}, \tag{10}$$

or form difference = size difference + shape difference. The size tensor simply measures the size difference at homologous points in the reference and target elements. Geometrically, it describes the average extent of radial expansion and/or contraction local to a point, so that a sphere in the reference element remains a sphere in the target element, varying only in its size. Algebraically, the size tensor is a constant (s) times an identity matrix (I):

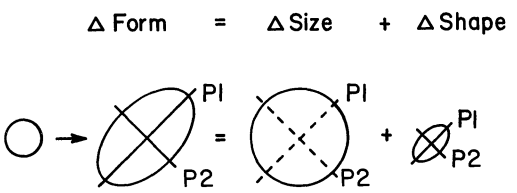

FIG. 9. Form tensor (**F**) can be divided into two additive tensors, a size tensor (**S**) and a shape tensor (**T**). Tensors figured graphically above. Circle to left of arrow represents reference region, while ellipse to right of arrow represents deformed region. Principal directions are P1 and P2. Principal directions are dashed on size tensor because all of its directions show equal strain and, thus, placement of principal directions is arbitrary.

$$\mathbf{S} = s\mathbf{I} = s\begin{bmatrix} 1 & 0 & 0 \\ 0 & 1 & 0 \\ 0 & 0 & 1 \end{bmatrix} = \begin{bmatrix} s & 0 & 0 \\ 0 & s & 0 \\ 0 & 0 & s \end{bmatrix}, \tag{11}$$

where s is the average normal strain, the average eigenvalue, or one-third the trace of **F**,

$$s = (n_x + n_y + n_z)/3. \tag{12}$$

The average normal strain (s) is invariant with respect to the coordinate system in which the tensor is described. Three times average normal strain (s) is usually referred to as the first invariant (Malvern, 1969) in continuum mechanics. We refer to it as size, since it measures size differences local to an identified point. This size measure is very highly correlated with differences in volume between target and reference elements (Cheverud et al., 1983).

The shape tensor (**T**) measures *variation* in radial expansion and/or contraction of different dimensions in the region immediately surrounding a point. Geometrically, it describes the change in this region from a sphere to an ellipsoid of equal size (volume) in going from the reference to the target element (see Fig. 9). Only shape changes are measured with size changes being held apart. Algebraically, the shape tensor (**T**) is

$$\mathbf{T} = \mathbf{F} - \mathbf{S},$$

$$\mathbf{T} = \begin{bmatrix} n_x & e_{xy} & e_{xz} \\ e_{yx} & n_y & e_{yz} \\ e_{zx} & e_{zy} & n_z \end{bmatrix} - \begin{bmatrix} s & 0 & 0 \\ 0 & s & 0 \\ 0 & 0 & s \end{bmatrix},$$

$$\mathbf{T} = \begin{bmatrix} n_x - s & e_{xy} & e_{xz} \\ e_{yx} & n_y - s & e_{yz} \\ e_{zx} & e_{zy} & n_z - s \end{bmatrix}. \quad (13)$$

The particular values of shape tensor elements vary depending on the coordinate system in which it is measured, but like the form tensor, simple tensor rotations allow mathematically equivalent expressions of the shape tensor in any coordinate system. Shape tensors should only be directly compared when they are expressed in the same coordinate system.

However, the *magnitude* of shape difference between reference and target elements in a region immediately surrounding the point of interest is invariant with respect to coordinate systems. Only the *pattern* of shape difference, which describes the directional or spatial configuration of variable expansion and/or contraction, depends on a coordinate system. The magnitude of shape difference is measured by the second invariant (II) of the shape tensor in continuum mechanics (Malvern, 1969). We have chosen a transformation of this second invariant to measure the magnitude of shape difference (t),

$$t = [(\tfrac{2}{3})\mathrm{II}]^{1/2}, \\ = [(\lambda^2_{T1} + \lambda^2_{T2} + \lambda^2_{T3})/3]^{1/2}. \quad (14)$$

This is computationally equivalent to the standard deviation of the principal values (eigenvalues [λ]) of the shape tensor and fits conceptually with the idea of shape differences as spatially varying size differences. It also provides a measure of the magnitude of shape difference (t) on the same scale as our measure of the magnitude of size difference (s). Thus, we can determine whether two regions differ more in size or in shape between the target and reference elements.

As noted above, the pattern of shape difference needs to be described within some coordinate system and cannot be reduced to a single number. However, two patterns of shape difference can be compared to one another using matrix correlations (Sokal and Sneath, 1972) between two tensors described in the same coordinate system. A high correlation indicates a strong similarity of pattern in the two tensors, independent of the magnitude of shape change expressed by each shape tensor. Fisher's z-transformations of such matrix correlations could be used in statistical analysis.

While the size (s) and shape (t) values refer to differences local to a given point, summary measures also are available. The average size ($\bar{s}$) and shape ($\bar{t}$) values over an element or form can be obtained by integration over all of the points contained within it (Lewis et al., 1980). A simpler, but perhaps slightly less accurate, method would be to average the s and t values obtained for every vertex of every element. By these means an average magnitude of size and shape difference over the whole form can be obtained.

Shape differences between two forms can also be considered at many levels. The local level was described above and is measured by t. Higher levels of shape difference between two forms may exist, even in the absence of localized shape differences. For example, in comparing an infant to an adult male rhesus macaque skull (see Fig. 5), magnitudes of local size difference (s) are much greater in the face than in the neurocranium, thereby identifying a shape difference between skulls at a more global level than measured by local shape (t). We suggest that the magnitude of this spatial variation in local size difference be measured by the standard deviation of local size differences,

$$tg = \left\{ \left[\sum_{i=1}^{n} (s_i - \bar{s})2 \right] / n \right\}^{1/2}, \quad (15)$$

as local shape (t) is measured by the standard deviation of size differences along the principal directions. This global shape difference measure could be produced at any of several levels of form subdivision, such as between points within subregions, between subregions within regions, and between regions within forms.

The measures described here seem rea-

sonable to us, but with experience other measures drawn from finite-element scaling may prove more useful. It is certainly true that the scheme of measurements described above is not the same as those used in previous statistical analyses by Cheverud et al. (1983) or Richtsmeier (1985). We may expect some future evolution in this new field.

SEXUAL DIMORPHISM IN RHESUS MACAQUE FACIAL GROWTH

We now present an example of the use of finite-element scaling in a preliminary analysis of sexual dimorphism in facial growth in *Macaca mulatta*. The three-dimensional coordinates of 42 homologous points were recorded on 249 rhesus macaque crania from the Cayo Santiago skeletal collection using a diagraph and then input to the computer with a graphics tablet (Cheverud et al., 1983). We have analyzed two contiguous elements representing the right upper and lower face using 12 points. Homologous points were measured on the right side of rhesus macaque faces. The numbers of the points correspond to those given in Cheverud et al. (1983): (1) intradentale superior; (2) alveolar junction of maxilla and premaxilla; (4) inferior pterygo-maxillary junction; (6) posterior nasal spine; (7) inferior internasal junction; (8) zygomaxillare superior; (10) superior border of the pterygopalatine fossa; (12) inferior vomer-sphenoid junction; (13) nasion; (16) fronto-malar junction; (18) spheno-fronto-malar junction; and (41) point midway between the posterior aspects of the orbits (near tuberculum sella). The elements analyzed here include numbers 1 and 3 from Figure 3 and in Cheverud et al. (1983). The lower face element is composed of points 8, 10, 12, 7, 2, 4, 6, and 1, while the upper face element contains points 16, 18, 41, 13, 8, 10, 12, and 7.

All of the crania were translated and rotated to a common localized coordinate system with the origin at the figure centroid, the anterior-posterior (A-P) axis running from intradentale superior to lambda, the medial-lateral (M-L) axis nearly parallel to a line connecting right and left pterion, and the superior-inferior (S-I) axis nearly colinear with a line connecting bregma and clivus. Yearly age- and sex-specific mean crania were generated using the average location of each point. Sample sizes (males, females) used to generate the average facial elements for each age group (number in parentheses is age in years) were (1) 7, 6; (2) 7, 11; (3) 9, 14; (4) 12, 12; (5) 12, 11; (6) 11, 3; (7+, adult) 52, 44. Given the relatively small size of some subadult samples, the following results should be taken to demonstrate general age-related trends. While such trends are probably robust, individual deviations from them should not be overinterpreted. All ages at death and sex identifications are known from the Cayo Santiago colony records (Sade et al., 1986) and thus need not be estimated using skeletal criteria.

We performed a cross-sectional study of sex-specific growth using finite-element scaling. Each age- and sex-specific mean was characterized relative to the average one-year-old male cranium. Thus, elements 1 and 3 taken from the average one-year-old male serve as reference elements which were then deformed into the homologous target elements of all other age- and sex-specific average crania. The results for points which occur in both elements are the average of individual element deformations.

RESULTS

Table 2 contains the local size differences (s) between the average one-year-old male face and all other age- and sex-specific means. Overall difference in facial size ($\bar{s}$) is measured by the average of local size differences. These averages are plotted against age in Figure 10 for both males and females. Adult males are about 118% larger, while adult females are only about 73% larger than one-year-old males, thus demonstrating the more extreme growth of males. The relationship between total size and age is approximately linear in each sex ($r^2 = 0.98$ in females and 0.99 in males) with males growing 0.197 size units per year and females growing 0.108 units.

TABLE 2. Local (s_i) and total ($\bar{s}$) size differences between reference face (average one-year-old male), and age- and sex-specific mean target faces. Also included are overall shape magnitude (tg) and individual-point growth rates (b).

Point	Age 1	2	3	4	5	6	7+	b
				Males				
1	.00	.15	.31	.55	.80	.98	1.21	.21
2	.00	.22	.53	.83	1.24	1.48	1.68	.30
4	.00	.25	.45	.74	1.03	1.32	1.69	.28
6	.00	.28	.25	.41	.55	.68	.74	.12
7	.00	.24	.34	.64	.88	1.03	1.14	.20
8	.00	.14	.38	.69	1.02	1.23	1.26	.24
10	.00	.16	.21	.32	.44	.56	.67	.11
12	.00	.18	.24	.28	.45	.58	.63	.10
13	.00	.17	.23	.48	.63	.66	.70	.12
16	.00	.28	.37	.50	.60	.63	.81	.12
18	.00	.31	.22	.70	1.06	1.13	1.19	.22
41	.00	.81	.83	1.09	1.35	1.93	2.45	.36
$\bar{s}$	.00	.27	.36	.60	.84	1.02	1.18	.20
tg	.00	.17	.17	.22	.29	.41	.52	
				Females				
1	−.02	.09	.25	.37	.48	.55	.80	.13
2	.02	.16	.43	.57	.70	.84	1.12	.18
4	.06	.23	.39	.59	.71	.66	1.17	.16
6	−.03	.13	.25	.30	.35	.30	.52	.08
7	.01	.15	.28	.40	.49	.58	.74	.12
8	.04	.19	.26	.40	.48	.59	.87	.13
10	−.01	.05	.18	.24	.27	.27	.44	.07
12	−.04	.05	.14	.18	.21	.24	.34	.06
13	−.01	.10	.23	.31	.39	.43	.50	.08
16	.03	.20	.36	.47	.52	.80	.55	.11
18	.13	.24	.36	.36	.37	.43	.75	.08
41	−.02	.22	.32	.29	.19	.68	.91	.13
$\bar{s}$	.01	.15	.29	.37	.43	.53	.73	.11
tg	.05	.07	.08	.12	.16	.19	.25	

Thus, the male face grows nearly twice as fast as the female face. Sex differences in the growth period's offset time appear minor. This is consistent with the relatively small sex differences noted in timing of dental eruption (Cheverud, 1981). An adult female is approximately the same size as a 4.5-year-old male.

The magnitudes of global shape differences (tg) relative to one-year-old males are measured by the standard deviations of local size differences (see Table 2). These standard deviations are plotted against age in Figure 11 for each sex. Adult males are twice as different in shape from one-year-old males ($tg = 0.522$) as adult females are ($tg = 0.254$). The magnitude of global shape differences increases nearly linearly in females ($r^2 = 0.97$) and in males ($r^2 = 0.94$), except that two- and three-year-old males are equally distinct in overall shape from the one-year-old average. Male shape deviates from the reference at a rate of 0.077 units per year, while female global shape changes at a rate of 0.034 units, or about half as fast. Adult females are as different from the reference in overall shape as 4.5-year-old males are.

The pattern of global shape divergence from the one-year-old male baseline is recorded as the change in size during growth at each individual point relative to growth in average size. It is reflected in variation in the growth rates of the regions surrounding individual points (see Table 2). Similarity of global shape among age- and

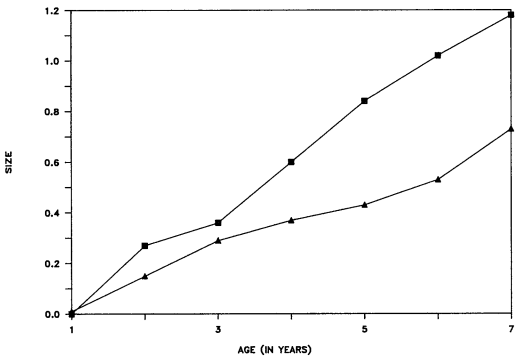

FIG. 10. Male and female growth curves for global facial size ($\bar{s}$; ■, male; ▲, female).

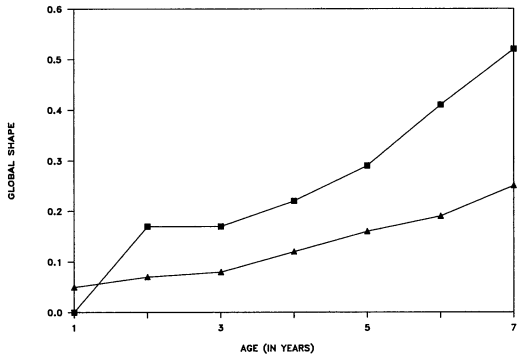

FIG. 11. Male and female growth curves for magnitude of global shape differences (tg; ■, male; ▲, female).

sex-specific mean faces is measured by the Pearson product-moment correlation between age- and sex-specific local sizes (see Table 3). Correlations tend to be low for age- and sex-specific means that do not differ much in shape from one-year-old males (one-year-old females and two-year-old males and females), indicating an indistinct pattern of shape change. By age 3, correlations of global shape patterns are high. A characteristic male facial shape can be discerned at age 2 and does not change after age 4.

The growth rates for individual points' local sizes (linear regression of s_i on age) are presented in Table 2 (column labeled b). Regions surrounding points which grow at higher than average rates account for a greater proportion of the face in older animals, thereby indicating the pattern of global shape change during growth. Points along the alveolus grow at high rates (pts. 1, 2, 4) as does point 41, midway between the posterior aspect of the right and left orbits. Point 41 is located near tuberculum sella on the anterior cranial base. Three points defining the nasal and maxillary sinus cavities, posterior nasal spine (pt. 6), superior pterygo-palatine fossa (pt. 10), and the vomer-sphenoid junction along the external cranial base (pt. 12), grow at particularly slow rates. Thus, expansion of the lower face is due primarily to localized growth along the alveolus (pts. 1, 2, 4) with relatively little growth posteriorly (pts. 6, 10, 12). In contrast, growth in the upper face is most extensive in the superior-posterior region (pts. 18, 41), followed by the inferior-anterior region (pts. 7, 8), the superior-anterior region (pts. 13, 16), and finally the inferior-posterior region (pts. 8, 10). This variation in growth

TABLE 3. Correlations between age- and sex-specific global shapes (M, male; F, female; number = age in years).

	M3	M4	M5	M6	M7	F1	F2	F3	F4	F5	F6	F7
M2	.80	.70	.55	.67	.73	−.07	.51	.29	−.11	−.38	.29	.25
M3		.86	.77	.86	.92	−.09	.54	.50	.31	.08	.67	.65
M4			.97	.98	.96	.33	.77	.70	.47	.24	.70	.82
M5				.97	.92	.42	.74	.72	.52	.33	.67	.87
M6					.98	.25	.67	.61	.40	.20	.61	.84
M7						.17	.65	.60	.40	.19	.63	.82
F1							.70	.65	.54	.44	.28	.44
F2								.83	.62	.39	.65	.68
F3									.67	.70	.82	.79
F4										.95	.81	.79
F5											.67	.68
F6												.73

TABLE 4. Magnitudes of local shape change (t) between reference face (average one-year-old male), and age- and sex-specific mean target faces.

Point	Age 1	2	3	4	5	6	7+
Males							
1	.00	.11	.17	.37	.54	.72	.96
2	.00	.15	.35	.65	.95	1.11	1.30
4	.00	.16	.30	.53	.69	1.00	1.42
6	.00	.45	.14	.22	.33	.46	.45
7	.00	.14	.16	.34	.46	.54	.65
8	.00	.16	.33	.60	.82	.86	.88
10	.00	.25	.15	.23	.29	.39	.49
12	.00	.10	.15	.17	.27	.35	.40
13	.00	.11	.21	.38	.57	.59	.64
16	.00	.35	.43	.59	.65	.65	.87
18	.00	.59	.26	1.00	1.30	1.34	1.46
41	.00	1.09	.85	.42	1.33	1.91	2.43
$\bar{t}$	.00	.30	.29	.46	.68	.83	1.00
Females							
1	.03	.11	.18	.30	.38	.50	.74
2	.05	.18	.30	.45	.51	.72	.93
4	.16	.24	.29	.42	.52	.46	1.02
6	.09	.12	.23	.17	.27	.39	.40
7	.03	.10	.16	.23	.27	.34	.45
8	.10	.22	.26	.37	.36	.54	.59
10	.09	.12	.17	.19	.20	.23	.38
12	.03	.08	.10	.12	.19	.19	.28
13	.03	.10	.15	.21	.24	.33	.36
16	.11	.31	.47	.57	.57	1.00	.52
18	.22	.40	.56	.54	.58	.61	.93
41	.06	.30	.40	.31	.17	.76	.89
$\bar{t}$	.08	.19	.27	.32	.35	.50	.62

rates at various element vertices indicates a complex shape change in the upper face during growth. These growth patterns are displayed graphically for midline points in the Thompson grids (see Fig. 5).

The pattern of female growth is generally similar to the pattern of male growth, especially as exemplified by adult females (see Tables 2, 3), although morphology differs in detail at any given age. The only important difference between the sexes in relative point-specific growth rates is at the spheno-fronto-malar junction on the lateral side of the orbit (pt. 18), which grows slowly in females compared to overall growth, but is about average in its growth in males. Thus, females generally follow the same pattern of overall shape change during growth as males, but achieve male shapes at later ages.

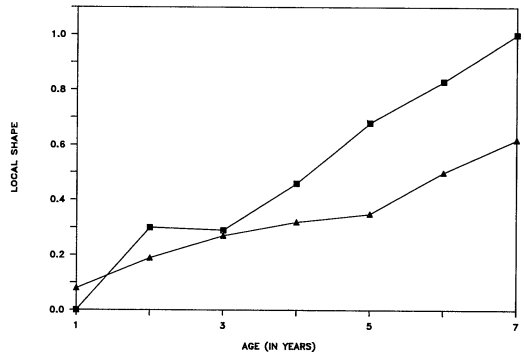

FIG. 12. Male and female growth curves for average magnitudes of local shape change ($\bar{t}$; ■, male; ▲, female).

The magnitude of shape change local to each point (t) is given in Table 4. The averages of these local shape values for each sex are plotted against age in Figure 12. Local shape change in males ($b = 0.156$) occurs at nearly twice the rate as in females ($b = 0.083$). Both plots are approximately linear ($r^2 = 0.97$ for both sexes), although local shape changes are not larger in three-year-old males than in two-year-olds. Points that show particularly large local shape changes during growth include the alveolar points (pts. 1, 2, 4), the spheno-fronto-malar junction (pt. 18), and the point midway between the posterior aspect of the orbits (pt. 41). These are also the points with the highest growth rates for local size (see above). Adult females have local shape magnitudes equivalent to those found in 4.75-year-old males.

In order to compare patterns of local

TABLE 5. Average correlations between local shape tensors (T) for age- and sex-specific means. Measures similarity of local shape patterns (male–male correlations above diagonal, female–female below diagonal, and male–female correlations on diagonal).

Male age	Female age 1	2	3	4	5	6	7+
2	.86	.89	.85	.87	.85	.84	.80
3	.79	.95	.97	.96	.96	.96	.92
4	.77	.94	.98	.99	.99	.99	.98
5	.74	.91	.96	.98	.97	.99	.99
6	.57	.84	.92	.92	.89	.89	.99
7+	.75	.92	.93	.96	.97	.92	.98

shape change between ages and sexes, matrix correlations were calculated between the age- and sex-specific shape tensors for each point. These correlations were then transformed to Fisher's Z-scores and averaged over points. The average was back-transformed to a correlation scale. Average correlations between local shape changes are presented in Table 5. All of the average correlations are very high except those involving one-year-old females ($\bar{r} = 0.57$–0.86), which show only small local shape differences from one-year-old males. Average correlations between males and females (along the diagonal) are especially noteworthy and very high. Particular points that tend to have low correlations include the vomer-sphenoid junction (pt. 12) in comparisons involving adult males and alveolar regions (pts. 2, 4) in comparisons involving six-year-old females. The canine and third molar are erupting adjacent to these alveolar points in six-year-old females, although the sample size is very small for this group.

The spatial pattern of local changes at particular points can be determined by examination of the shape tensors (which are available from the authors upon request). Local morphological changes can be detected with these shape tensors. While the typical shape change at the alveolar junction of pterygoid and maxilla (pt. 4) involves disproportionate expansion superior-inferiorly, six-year-old females show disproportionate anterior-posterior expansion as the third molar erupts in this region. Typical shape change at the alveolar premaxilla-maxilla junction involves disproportionate change anterior-posteriorly. Six-year-old females are disproportionately large superior-inferiorly. Thus, as the canine is erupting, the finite-element method seems to identify these local morphological changes related to dental eruption.

In general, over all of the points, local expansion during facial growth as indicated by the shape tensors is greatest in a general anterior-posterior direction, followed by the superior-inferior direction with disproportionately little growth medial-laterally. This pattern is followed by half of the points (1, 2, 7, 10, 12, 13), whose shape tensors show high across point intercorrelations ($\bar{r} = 0.84$).

The direction of greatest expansion for most points runs in an anterior-superior to posterior-inferior direction. Note that this contrasts with the usual description of facial growth as anterior-inferior. The anterior-inferior description is relative to the cranial base and is not descriptive of intrinsic facial growth. Exceptional points include: (1) zygomaxillare superior (pt. 8) that shows disproportionately large medial-lateral expansion, presumably relating to the flaring of the zygomatic arch during growth; (2) inferior pterygo-maxillary junction (pt. 4) that expands disproportionately in a superior-inferior direction as the permanent molars erupt; (3) posterior nasal spine (pt. 6) and the frontomalar junction (pt. 16) that show disproportionately little growth superior-inferiorly; and (4) the point midway between the posterior aspects of right and left orbits (pt. 41) and spheno-fronto-malar junction on the external orbit (pt. 18) that show strongly disproportionate growth in an anterior-inferior to posterior-superior direction. Thus, the commonly observed anterior-inferior displacement of the face relative to the neurocranium may be due largely to growth in the anterior cranial base region.

DISCUSSION

Heterochrony refers to a change in the timing or rate of growth in size and shape (Gould, 1977; Alberch et al., 1979). The finite-element method provides a way of separately measuring the fundamental parameters of heterochrony. Previous suggestions that a ratio of some chosen character to overall size be used as a measure of shape (Alberch et al., 1979) are unsatisfactory, since they lead to a mathematical confounding of size and shape (Atchley et al., 1976). Shape metrics (t, tg) of finite-element scaling are mathematically independent of size, although they retain the desirable possibility of remaining biologically correlated with it. This is unlike

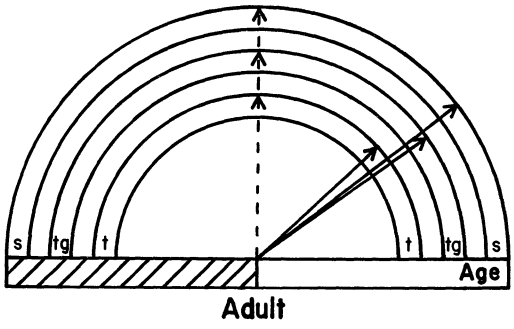

FIG. 13. Clock model (Gould, 1977) describing heterochronic transformation from female to male morphology. Process displayed is rate hypermorphosis (Shea, 1983). Dial *s* is for size, *tg* for overall shape, and *t* for local shape. Bar at bottom represents age, solid arrows indicate adult males, and dashed arrows indicate adult females.

measuring shape using residuals from regressions of single characters on size which produce only size-free shape metrics eliminating shape which is correlated to size.

The description of male and female facial growth given above allows a heterochronic description of sexual differences in morphology. First, male and female facial growth seem very similar morphologically. Males merely carry a common growth pattern to a further extent than females do. This is accomplished by male size and shape growing at nearly twice the rate of females, with relatively little apparent difference in the timing of growth offset in our preliminary analyses.

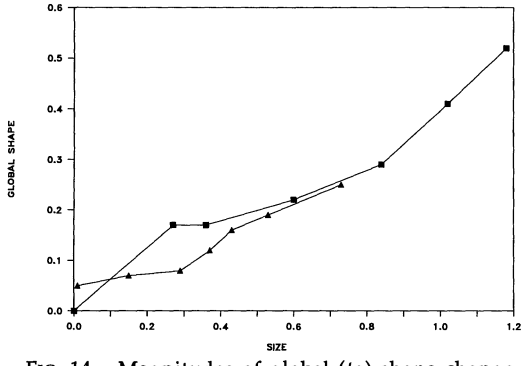

FIG. 14. Magnitudes of global (*tg*) shape change relative to size change during growth for males and females (■, male; ▲, female).

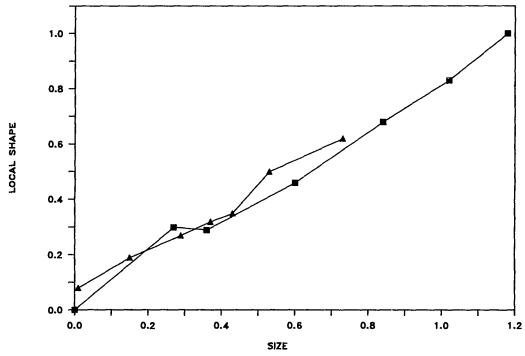

FIG. 15. Magnitudes of local ($\bar{t}$) shape change relative to size change during growth for males and females (■, male; ▲, female).

Adult females are nearly identical morphologically to four- to five-year-old males. They have the same overall size as these juvenile males and have the same magnitude of global and local shape distinction from one-year-old males. Furthermore, the pattern of shape difference from one-year-old males is the same for juvenile males and adult females (global shape pattern, $r = 0.85$; average local shape pattern, $\bar{r} = 0.97$). Direct finite-element comparisons of adult females to four- and five-year-old males support the lack of significant morphological distinctions between them.

Thus, in heterochronic terms, taking female morphology as primitive, males have a peramorphic morphology with both size and shape beyond those obtained by females. Furthermore, given the nearly equal offset times for male and female facial growth, this peramorphosis is due specifically to rate hypermorphosis (Shea, 1983), in which the rate of growth for both size and shape increases proportionately in the descendant form with little change in the time of growth offset. A clock model (Gould, 1977) for this heterochronic transformation is presented in Figure 13 with hands for size ($\bar{s}$), overall shape (*tg*), and local shape (*t*). There is little or no dissociation of size and shape involved in the female to male change. Finite-element scaling seems an ideal method for identifying and classifying heterochronies.

Strain parameters derived from finite-

element scaling can also be used in allometry, or the study of size-related changes in shape (Gould, 1966). This is typically done by regressing some part of an organism on its overall size after logarithmic transformation. The residuals can in some sense be considered as size-free shape measures. The same procedure could be followed by regressing local sizes (s_i), or strain in some specified direction, on overall size ($\bar{s}$) (Cheverud et al., 1983). In addition, the magnitude of shape change (t or tg) could be regressed on size for a direct analysis of the relationship between size and shape.

For the present growth data, size is very highly correlated with both global and average local shape magnitudes ($r > 0.95$ in both sexes). Also, the relationship between size and shape is the same in both sexes with a regression slope of 0.3 to 0.4 for global shape and 0.75 to 0.80 for local shape measures (see Figs. 14 and 15, respectively). It is easily seen, from the plots in Figures 14 and 15 and the evidence presented above indicating similar shape patterns in males and females, that adult male faces are allometrically scaled-up versions of adult female faces. Furthermore, since the shape-on-size regression slopes are significantly greater than zero, there is significant overall allometry, or deviation from isometry. Regions that are positively and negatively allometric were identified as growing particularly fast or slow in the Results section (Table 2, column labeled b). As its name suggests, finite-element scaling is a powerful measurement tool in scaling or allometry analyses.

As can be gathered from the discussion of allometry above, size grows faster than shape in rhesus macaque faces. Shape changes occur more rapidly and are more extensive locally than globally, indicating that various morphological dimensions, such as anterior-posterior or medial-lateral, show more variation in their growth than do the various regions of the face. We also discovered that there is great heterogeneity from point to point in both the magnitude and pattern of growth. Heterogeneity in magnitudes of local growth was measured by global shape change. The average correlation of shape tensors between points within a face was low ($r_{max} = 0.26$). However, several points (pts. 1, 2, 7, 10, 12, 13) did show a common pattern of local shape change.

While studies of facial growth in registered systems often describe the face as growing down and out, we find that this movement of points is most likely due to growth in the superior-posterior region of the face and anterior cranial base (pts. 18, 41) rather than a common feature of intrinsic facial growth. Most facial points show disproportionately large growth in a posterior-inferior to anterior-superior direction with considerable but lower growth magnitudes in posterior-superior to anterior-inferior directions. Thus, intrinsic facial growth or transformation can be very different from the displacement of facial points due to growth at the anterior cranial base, or translation (Enlow, 1966; Duterloo and Enlow, 1970).

We believe that finite-element scaling solves many outstanding and often unrecognized problems inherent in earlier means of measuring and comparing forms. Its main advantage is its ability to localize differences between forms and allow the retention of three-dimensional spatial pattern in statistical analyses of morphology. Finite-element scaling literally allows quantification of Thompson grids. While engineering and biomechanical applications of finite-element analysis are commonplace, its use in studies of ontogenetic and evolutionary morphological transformations has just begun. Thus, we can expect much growth and development in the application of finite-element analysis to morphological problems.

ACKNOWLEDGMENTS

We extend our thanks to Larry Cochard and Brian Shea for their comments on an earlier version of this paper, to Robert Hanmer for his help in programming, and to Karen Hanmer for drafting most of the figures. We give special thanks to Jack Lewis, without whose help this project could not have been completed. This research was generously supported by a

Biomedical Research Grant from the Whitaker Foundation.

REFERENCES

ALBERCH, P., S. J. GOULD, G. OSTER, AND D. B. WAKE. 1979. Size and shape in ontogeny and phylogeny. Paleobiology, 5:296–317.

ATCHLEY, W. R., C. T. GASKINS, AND D. ANDERSON. 1976. Statistical properties of ratios. I. Empirical results. Syst. Zool., 25:137–148.

BOOKSTEIN, F. L. 1978. The measurement of biological shape and shape change. Lecture Notes in Biomathematics, No. 24. Springer-Verlag, New York.

BOOKSTEIN, F. L. 1983. The geometry of craniofacial growth invariants. Am. J. Orthod., 83:221–234.

BOOKSTEIN, F. L. 1984a. A statistical method for biological shape change. J. Theor. Biol., 107:475–520.

BOOKSTEIN, F. L. 1984b. Modeling differences in cranial form, with examples from Primates. Pages 207–229 *in* Size and scaling in primate biology (W. L. Jungers, ed.). Plenum Press, New York.

BOOKSTEIN, F. L., B. CHERNOFF, R. ELDER, J. HUMPHRIES, G. SMITH, AND R. E. STRAUSS. 1985. Morphometrics in evolutionary biology. Spec. Publ. 15, Academy of Natural Sciences, Philadelphia.

CHEVERUD, J. M. 1981. Epiphyseal union and dental eruption in *Macaca mulatta*. Am. J. Phys. Anthropol., 56:157–168.

CHEVERUD, J. M., J. L. LEWIS, W. BACHRACH, AND W. B. LEW. 1983. The measurement of form and variation in form: An application of three-dimensional quantitative morphology by finite-element methods. Am. J. Phys. Anthropol., 62:151–165.

DUTERLOO, H. S., AND D. H. ENLOW. 1970. A comparative study of cranial growth in *Homo* and *Macaca*. Am. J. Anat., 127:357–368.

ENLOW, D. H. 1966. A morphogenetic analysis of facial growth. Am. J. Orthod., 52:283–299.

ENLOW, D. H. 1975. Handbook of facial growth. W. B. Saunders Co., Philadelphia.

GOULD, S. J. 1966. Allometry and size in ontogeny and phylogeny. Biol. Rev., 41:587–640.

GOULD, S. J. 1977. Ontogeny and phylogeny. Harvard Univ. Press, Cambridge, Massachusetts.

GRAYSON, B., N. WEINTRAUB, F. L. BOOKSTEIN, AND J. MCCARTHY. 1985. A comparative cephalometric study of the cranial base in craniofacial anomalies: Part I: Tensor analysis. Cleft Palate J., 22:75–87.

LESTREL, P. E. 1974. Some problems in the assessment of morphological size and shape differences. Yrbk. Phys. Anthropol., 18:140–162.

LEW, W. B., AND J. L. LEWIS. 1977. An anthropometric scaling method with application to the knee joint. J. Biomech., 10:171–181.

LEWIS, J. L., W. B. LEW, AND J. L. ZIMMERMAN. 1980. A nonhomogeneous anthropometric scaling method based on finite element principles. J. Biomech., 13:815–824.

MALVERN, L. 1969. Introduction to the mechanics of a continuous medium. Prentice-Hall, New Jersey.

MCMAHON, T., AND J. T. BONNER. 1983. On size and life. W. H. Freeman and Co., New York.

MEDAWAR, P. B. 1958. D'Arcy Thompson and growth and form. Pages 157–183 *in* D'Arcy Wentworth Thompson: The scholar-naturalist (R. D'Arcy Thompson, ed.). Oxford Univ. Press, London.

MOSIMANN, J. E. 1970. Size allometry: Size and shape variables with characterizations of the log-normal and generalized gamma distributions. J. Am. Stat. Assoc., 65:930–945.

MOSIMANN, J. E., AND F. C. JAMES. 1979. New statistical methods for allometry with application to Florida red-winged blackbirds. Evolution, 33:444–459.

MOSS, M. L. 1983. Beyond roentgenographic cephalometry—What? Am. J. Orthod., 84:77–79.

MOSS, M. L., R. SKALAK, G. DASGUPTA, AND H. VILMANN. 1980. Space time and space-time in craniofacial growth. Am. J. Orthod., 77:591–612.

MOSS, M. L., R. SKALAK, H. PATEL, K. SEN, L. MOSS-SALENTIJN, M. SHINOZUKA, AND H. VILMANN. 1985. Finite element method modeling of craniofacial growth. Am. J. Orthod., 87:453–472.

MOYERS, R. E., AND F. L. BOOKSTEIN. 1979. The inappropriateness of conventional cephalometrics. Am. J. Orthod., 75:599–617.

PATEL, H. 1983. Growth analysis by non-linear continuum theory. Doctoral Thesis, Columbia Univ., New York.

PEARSON, K., AND A. G. DAVIN. 1924. On the biometric constants of the human skull. Biometrika, 16:328–363.

RICHTSMEIER, J. T. 1985. A study of normal and pathological craniofacial morphology and growth using finite element methods. Doctoral Thesis, Northwestern Univ., Evanston, Illinois.

RICHTSMEIER, J. T., AND J. M. CHEVERUD. 1986. Finite element scaling analysis of human craniofacial growth. J. Craniofacial Gen. Develop. Biol., 6 (in press).

RIEDL, R. 1978. Order in living organisms. J. C. Wiley and Sons, New York.

SADE, D. S., B. D. CHEPKO-SADE, J. M. SCHNEIDER, S. S. ROBERTS, AND J. T. RICHTSMEIER. 1986. Basic demographic observations on free-ranging rhesus monkeys. Human Relations Area Files, Multimedia Publications, New Haven, Connecticut.

SHEA, B. T. 1983. Allometry and heterochrony in the African apes. Am. J. Phys. Anthropol., 62:275–289.

SKALAK, R., G. DASGUPTA, M. L. MOSS, E. OTTEN, P. DULLEMEIJER, AND H. VILMANN. 1982. Analytical description of growth. J. Theor. Biol., 94:555–577.

SNEATH, P. H. A. 1967. Trend surface analysis of transformation grids. J. Zool., Lond., 151:65–122.

SOKAL, R. R., AND P. H. A. SNEATH. 1972. Numerical taxonomy. W. H. Freeman and Co., San Francisco.

SPRENT, P. 1972. The mathematics of size and shape. Biometrics, 28:23–27.

STRAUSS, R. E., AND F. L. BOOKSTEIN. 1982. The truss: Body form reconstructions in morphometrics. Syst. Zool., 31:113–135.

THOMPSON, D'A. W. 1917. On growth and form. Cambridge Univ. Press, Cambridge.

Received 21 November 1985; accepted 28 May 1986.